Slow light structure with enhanced delay–bandwidth product

Kadir Üstün[1,2,*] and Hamza Kurt[2,3]

[1]*Department of Electrical and Electronics Engineering, Middle East Technical University, 06800 Ankara, Turkey*
[2]*Department of Electrical and Electronics Engineering, TOBB University of Economics and Technology, 06560 Ankara, Turkey*
[3]*e-mail: hkurt@etu.edu.tr*
**Corresponding author: k.ustun@etu.edu.tr*

Received February 22, 2012; revised July 10, 2012; accepted July 10, 2012;
posted July 11, 2012 (Doc. ID 163350); published August 15, 2012

In this study, we propose a special type of slow light photonic crystal (PC) waveguide structure to achieve slow light with an improved delay and bandwidth product (DBP). The waveguide is based on a triangular lattice PC with a line defect imposed by changing the radii and locations of the holes lying along the waveguide centerline. By altering the locations of these central holes, group indices ranging approximately from 25 to 40 are obtained over frequency intervals, attaining a nearly constant group index. It is also observed that the group index spectrum has an *S*-like shape under certain circumstances. The manipulations of structural parameters easily allow attaining higher or lower group indices. For special configurations, normalized DBPs can be enhanced up to a value of 0.554. According to the best of the authors' knowledge, this value is the highest value achieved with PC waveguide structures, and this value is achieved without using any special optimization methods such as topology optimization. Group velocity dispersion values of various configurations are minimized to enable proper optical pulse propagation.

OCIS codes: 130.5296, 230.5298, 130.2790, 260.2030.

1. INTRODUCTION

Since the first proposal of photonic bandgap materials [1,2], the photonic crystal (PC) concept has become a widespread research discipline [3]. Tailoring spatial profiles of the guided mode in PC waveguides by means of structural manipulations makes it possible to obtain a low group velocity of optical pulses. Slow light research strongly associated with dispersion engineering has recently regained vitality, and several research groups have been involved with this topic [4]. In general, slow light approaches can be broadly categorized into two groups, structural dispersion and material dispersion [4]. The target of the present work falls into the category of the first approach. The importance of slow light arises due to all-optical signal processing demand. Storing and reshaping of optical pulses are indispensable in this context. In addition, the enhancement of linear and nonlinear optical effects is promoted due to a longer interaction of the slow wave with the materials.

A large number of researchers have pursued slow light on PC-type structures. In most of the slow light photonic structures, a waveguide is obtained in terms of a line defect obtained by removing either holes or dielectric rods. Then slow light is achieved by tuning the structural features in the neighborhood of the line defect in various ways [5–21]. Briefly reviewing some of these studies, the tuning methods proposed previously can be summarized as follows: changing hole locations and diameters [5,7,8], chirping with two line defects [9], and inducing coupled cavities into photonic structures [10,11]. In addition to these approaches, reducing the waveguide width [12], changing the shape of holes [13], using microfluidic infiltration [14], and implementing polyatomic unit cells, asymmetric waveguides, and chirped coupled waveguides were also considered [16–18]. A general recipe was outlined in [22]. Moreover, one of the latest studies proposes a design with infiltrated holes that achieves high normalized delay and bandwidth product (DBP) and small group velocity dispersion (GVD) values [23]. Finally, another approach proposed recently is based on an automated design with topology optimization algorithms [24,25].

In this study, we first induce a line defect in a two-dimensional (2D) triangular lattice PC by decreasing the diameters of consecutive holes instead of completely removing them. We next change the defect holes' positions in the guiding (longitudinal) direction to obtain the desired dispersion diagram of the relevant guided mode. Then, we investigate the effects of the diameter of the hole and the change of the position of the hole in the transverse direction to propagation. At the end of these steps, we achieve a normalized DBP value of 0.554 where such a high value can only be achieved by special optimization procedures [24,25]. Furthermore, GVD performances of different cases are also discussed in the present work. We believe the outputs of the current research will provide important viewpoints about how to manipulate PC waveguide parameters for slow light purposes.

It is known that slow light study based on a structural dispersion mechanism heavily uses wavelength-scale modulation of the parameters that constitute the underlying PC. The usual starting point to obtain a PC waveguide is the removal of the central row of holes. Then the effects of the nearest neighbor rows are explored. Instead of following this approach, we keep the central row of holes, expecting that the light interaction with them will be more influential than other rows of

neighbor holes. We will show later in the paper that tuning the radii and locations of the holes residing along the waveguide centerline is an ideal alternative for cultivating the group velocity and dispersion features of optical pulses. Additionally, a unique property of the proposed waveguide configuration is the strong field localization in the air holes at the center region. These centralized holes can be filled with microfluidics or nonlinear materials. In this way, the sensitivity of biochemical sensors and the efficiency of nonlinear optical processes can be enhanced.

2. STRUCTURE AND NUMERICAL ANALYSIS

The investigated photonic structure consists of air holes in a dielectric background. The periodic pattern is created in terms of a triangular lattice formation. The relative permittivity of the background is 12. The radius of each hole is $r = 0.30a$, except the ones that occupy the centerline, where a is the lattice constant. The holes lying along the centerline constitute the waveguide. The radii and positions of these holes on the centerline are modified for design purposes. A sample PC waveguide is shown in Fig. 1. The waveguide is initially obtained by changing the radius of each defect to $R = 0.25a$ and shifting each defect by $0.462a$ in the x direction (ΓK). The structure behavior's dependence on the defect radius and position is analyzed afterwards. Different variations of this configuration are examined numerically by the plane wave expansion (PWE) method [26] with a grid size of $a/80$ in 2D. The band diagram of the initial case for the TE mode (h-field is in z direction) is shown in Fig. 2(a). The band to be engineered is shown with a thick dashed curve. The frequency region of interest stays under the light curve and close to lower edge of the bandgap zone. In fact, this band is an upshifted version of one of the dielectric continuum states of the original structure. The frequencies outside the bandgap are not considered due to lack of a waveguiding mechanism. The h-field distribution of the relevant band at $k_x = 0.5(2\pi/a)$ is shown in Fig. 2(b). The bandgap guiding of the mode is apparent in the figure. The mode with an even-type profile strongly focuses in the middle, where manipulated holes exist. In the following sections, we will change the structural parameters to achieve low GVD and a high normalized DBP in three optimization steps.

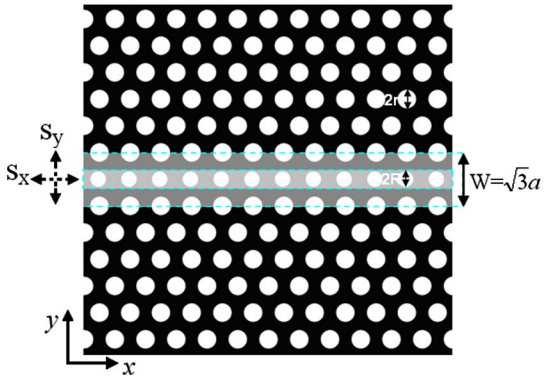

Fig. 1. (Color online) Schematic representation of a triangular lattice photonic crystal waveguide. The central row of holes is moved along the x and y directions. Additionally, the radii of these holes are tuned during the optimization steps presented in Section 2.

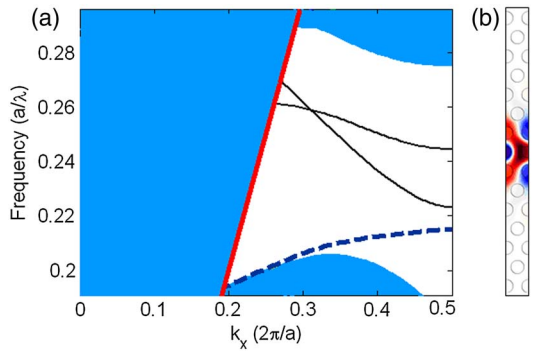

Fig. 2. (Color online) (a) Dispersion diagram for initial set of parameters ($S_x = 0.462a$, $S_y = 0$, and $R = 0.25a$). The band engineering is performed on the dashed cuve; (b) The h-field distribution of the mode at $k = 0.50(2\pi/a)$. The figure shows that the light is confined in the center region, verifying a waveguide formation.

A. Optimization Step 1: Longitudinal Perturbations

The first optimization step deals with the positions of the holes along the x direction. The shift of the hole (S_x) in the x direction is scanned in the interval of $[0.45a, 0.47a]$. The dispersion curves of the relevant modes are shown in Fig. 3(a). The gray line is the lower limit of the bandgap region. The bands span a large k-portion with small slopes and linear shapes. To reveal the slow light behavior of these linear

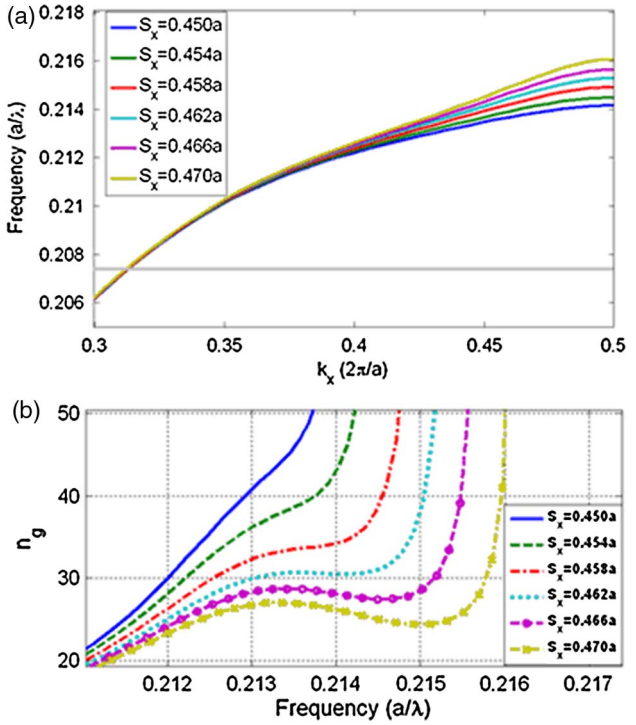

Fig. 3. (Color online) (a) Change in dispersion diagram with respect to various S_x values. S_y and R remain constant at 0 and $0.25a$, respectively. The lower bandgap limit is shown by the straight line at the lower part of the figure. Linear parts of the dispersion curves have an exceptional importance while achieving slow light with a low group velocity dispersion; (b) The calculated group index spectra of the band diagrams shown in (a). At $S_x = 0.458a$, a dispersion diagram with a chair shape is formed. That is, GVD tends to zero at frequencies near $\frac{a}{\lambda} = 0.2137$. Exceeding this S_x value, an S-like shape is added to the constant part of the chair shape. The local minima and maxima of this S shape exhibit zero GVD.

sections, the group index (n_g) of each case is calculated numerically and demonstrated in Fig. 3(b). The group index spectra show almost-constant group index regions with small intervals of change within the parameter interval of $S_x \in [0.458a, 0.466a]$. These constant group indices change from 35 to 24 and relevant frequencies shift to higher values as S_x increases within the specified interval. The decrease in the group index produces enhancement in the bandwidth that shows constant group index behavior. This usual phenomenon was revealed by previous studies [8]. The group index spectrum of the case $S_x = 0.458a$ shows nearly zero GVD in the normalized frequency interval of [0.2136, 0.2138]. If the shift is increased to values higher than $0.458a$, the group index spectrum shows an S-shape, with two points where GVD becomes zero. On the other hand, GVD has a finite and small value at the center of the S-shaped curve.

Another aspect of the group index spectra is that the frequency regions that show constant group velocity exhibit small deviations if the geometrical configuration does change in an interval of $\Delta x = \pm 0.004a$. This corresponds to a variation of approximately ± 1.328 nm if the lattice constant a is adjusted to be 332 nm. For the sake of brevity, we here choose $S_x = 0.462a$ to use a high bandwidth with low GVD so that we can proceed to the next stage of the optimization.

B. Optimization Step 2: Transverse Perturbations

In the second stage, we carry out optimizations for the shifts of holes in the y direction in the case $S_x = 0.462a$. The holes are shifted in the y direction within an interval of $S_y \in [0, 0.06a]$. The band behavior and group index spectrum are investigated. The dispersion diagram of each case is not shown because the bands are tightly spaced. In that case, we only show the group index spectra for different y shifts in Fig. 4. As can be seen from the figure, the frequency intervals that attain constant group indices exhibit almost no shift when we change the S_y parameter. There is a small amount of group index change as S_y deviates from zero. Namely, a shift of $\pm 0.02a$ (corresponding to ± 6.64 nm if a equals to 332 nm) does not significantly shift the group index value (negative shifts and positive shifts show the same dispersion diagrams because of the symmetry). Increasing the shift to higher values gives the slope a chair shape. All in all, we keep the S_y parameter as zero and continue with the third step of the optimization.

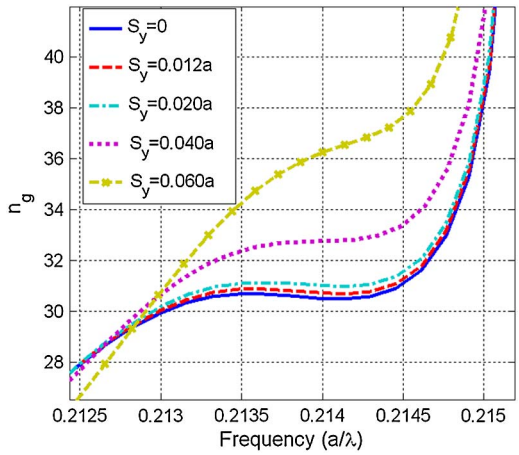

Fig. 4. (Color online) Change in group index spectra with respect to various S_y values. S_x and R remain constant at 0.462 and $0.25a$, respectively. At lower values of S_y, the deviation in the curve is very small.

C. Optimization Step 3: Filling Factor Variation

In the final step of the optimization, we play with the radii of the defect holes. The radius of the defect hole (R) is scanned within the interval of [$0.242a$, $0.258a$]. The band diagrams and the group velocity spectra are shown in Figs. 5(a) and 5(b), respectively. The dispersion curves show linear behavior, and the group index spectra show constant group index regions accordingly. The group index decreases from 50 to 24 with an increase in bandwidth as the radius of the center hole increases. The group index of a single band can be approximated by $n_g \approx c\frac{\Delta k}{\Delta \omega}$, where $\Delta k = k_2 - k_1$ and $\Delta \omega = \omega_2 - \omega_1$. The decrease in the group index is accounted for by the fast increase of the upper frequency limit ω_2 at roughly around $k_2 = 0.5\frac{2\pi}{a}$, compared to the lower frequency limit ω_1 that stays almost constant in the vicinity of approximately $k_1 = 0.35\frac{2\pi}{a}$. The wave vector interval exhibits small changes as the curves move to higher frequencies. As a result the ratio defined above allows the group index to decrease. The fast movement of the dispersion curve at the $k_2 = 0.5\frac{2\pi}{a}$ point is due to a decrease of the average dielectric constant at the waveguide centerline. It should be noted that the high symmetry points are more sensitive to structural changes in R. This can also be a result of the high symmetry in the fields. The constant group index regions deviate slightly in frequency while changing the radius in steps of $0.002a$ (corresponding to a 1.328 nm change in diameter). The group index also does

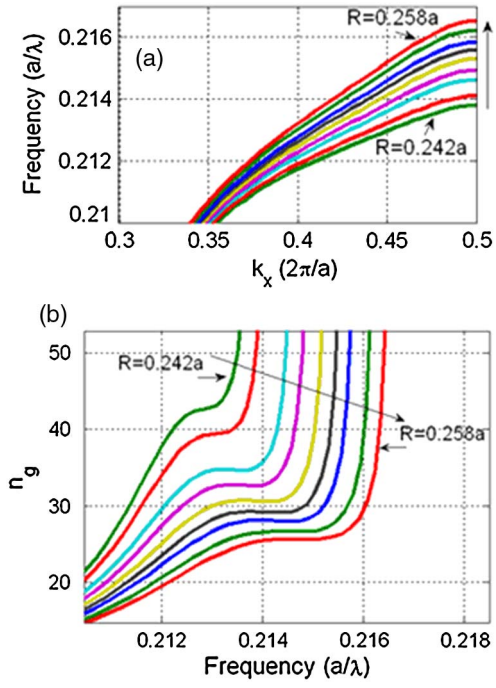

Fig. 5. (Color online) (a) Region of interest of the dispersion diagrams corresponding to various R values. S_x and S_y remain constant at $0.462a$ and 0, respectively. R values are scanned with a step size of $0.002a$. The linear parts of the dispersion diagram near $k_x = 0.45\frac{2\pi}{a}$ can be engineered to attain slow light; (b) The group index spectra of the dispersion curves. The chair shape is preserved with low GVD characteristics.

not deviate too much, especially if the mean value of R is chosen properly.

3. HIGHER ORDER DISPERSION ANALYSIS

Following the commonly accepted approach in slow light studies [23,27], the operation of the proposed structure is evaluated by its second (GVD) and third order dispersion (TOD) properties. The second order dispersion is expressed by GVD $= \partial^2 k/\partial\omega^2$, and it represents the wavelength dependency of the group index. TOD is computed by TOD $= \partial^3 k/\partial\omega^3$, and it is an indication of the wavelength dependency of GVD. These are directly calculated by the numerical differentiations of the dispersion curves. The GVD and TOD are shown in Figs. 6 and 7 in terms of normalized units of $a/2\pi c^2$ and $a^2/4\pi^2 c^3$, respectively. We demonstrate GVD for different cases of optimization in Fig. 6, where Figs. 6(a), 6(b), and 6(c) correspond to Optimization Steps 1, 2, and 3, respectively. The TOD of different cases is depicted in Fig. 7, where Figs. 7(a), 7(b), and 7(c) correspond to Optimization Steps 1, 2, and 3, respectively. GVD can be taken as a measure of the group index difference between different frequency components of the input pulse. A high GVD value is detrimental for optical pulses because of the distortion imposed on the pulse propagation. This is due to the fact that some part of the pulse is traveling faster than the other parts. In the limiting case, the information coded in the pulse would be lost, as the pulse peak will be too small to be detected as a result of pulse broadening in the time domain. Consequently, GVD puts a bottleneck to the bit rate speed of optical communication. In light of these arguments, it is of prominent importance to decrease the GVD values to avoid the aforementioned distortion effects. In most cases shown in Fig. 6, there are two points that cross the zero line. The GVD values between these two zero crossings stay very small. This shows that the structure proposed is an effective structure that can carry optical information with negligible distortion for a reasonably long propagation distance. The effect of TOD on the optical pulse is changing the shape of the optical dispersed signal, and it is inherent

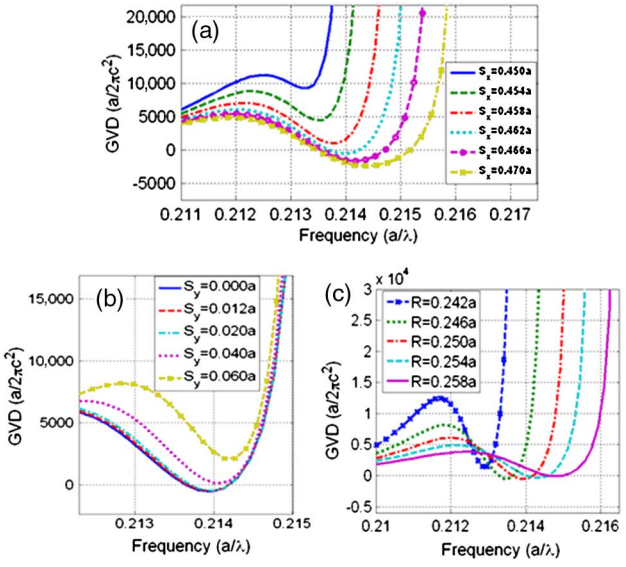

Fig. 6. (Color online) (a)–(c) GVD values for Optimization Steps 1, 2, and 3, respectively.

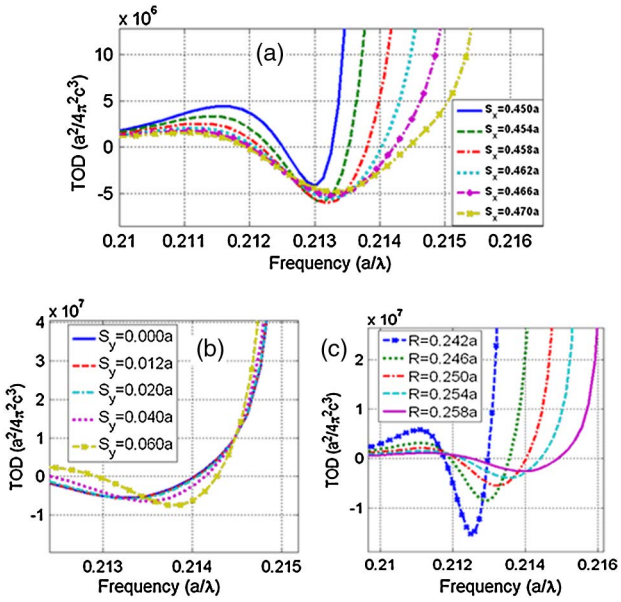

Fig. 7. (Color online) (a)–(c) TOD values for Optimization Steps 1, 2, and 3, respectively.

in the GVD parameter. As long as GVD is low enough, the TOD effect on the pulse shape is expected to be limited.

4. DELAY–BANDWIDTH PRODUCT CRITERIA

One of the key issues of slow light is the available bandwidth ($\Delta\omega/\omega_c$) that exhibits a nearly constant group index region. However, the bandwidth should also be considered together with the group index value. Hence, a figure of merit called the normalized DBP is introduced as $\langle n_g\rangle \times \Delta\omega/\omega_c$. The normalized DBP has a crucial effect; it is strongly related to the amount of bits that can be buffered in an optical element of finite length [28–30]. Therefore, the fidelity of most of the slow light structures is considered with respect to normalized DBP merit. The recently reported normalized DBP value of 0.406 belongs to a configuration that is made of PC waveguides without utilizing any optimization algorithm [23]. The slow light performance of different approaches in terms of normalized DBP values is compared in [31].

Here we also calculate the normalized DBP of the proposed structure. The baseline for determining the corresponding bandwidths is ±10% of the maximum change of the group index with respect to the center value. This convention is compatible with the literature. The normalized DBP dependencies on structure parameters S_x (for $S_y = 0$, and $R = 0.25a$) and R (for $S_x = 0.462a$ and $S_y = 0$) are given in Figs. 8(a) and 8(b), respectively. The values in the figure are extracted from the results of the optimization steps in Section 2. A constant increase in the normalized DBP is observed in Fig. 8(a). The maximum normalized DBP product of 0.441 is achieved with a set of parameters: $S_x = 0.470a$, $S_y = 0$, and $R = 0.25a$. The normalized DBP function of the structure with respect to the R parameter is investigated in Fig. 8(b). There is an increase in the normalized DBP, but it saturates at around 0.345 for large R values. It is also realized that $S_x = 0.462a$ is not the optimal value for optimizing the normalized DBP, in spite of its low GVD characteristics. The constant increase in the normalized DBP in Fig. 8(a) shows that there is already much room for

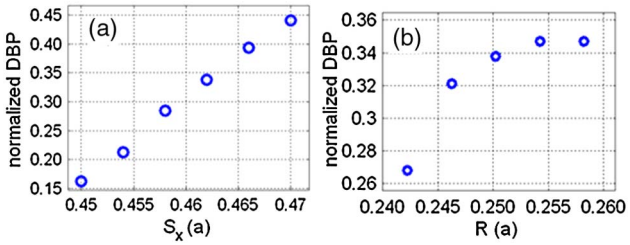

Fig. 8. (Color online) (a) Normalized DBP values that correspond to different S_x values. The other optimization parameters are kept at $S_y = 0$ and $R = 0.25a$. The highest normalized DBP reaches up to 0.441; (b) The normalized DBP values that correspond to different R values. The remaining parameters are fixed at $S_x = 0.462a$ and $S_y = 0$.

further optimization. It can be inferred from Fig. 8(b) that even $R = 0.25a$ cannot be considered as a general maxima point. Therefore, we continued our search for the maximum normalized DBP with the ±10% criteria. Individual steps of this search are not presented for brevity, but the results are presented in the discussion part.

5. DISCUSSION

As we calculate the bandwidth with a criteria of 10% change of the center group index (as used in previously published articles), we find that the highest normalized DBP attained within the optimization procedure presented above is 0.441 for the case of $S_x = 0.470a$, $S_y = 0$, and $R = 0.25a$. This value is higher than any value reported by previous studies. Furthermore, this structure consists of only two different materials, and this makes the present structure easy to manufacture. On the other hand, some studies depend on structures that consist of more than two different materials to improve the normalized DBP. The same methodology can be applied in our case as well.

We should point out that the GVD attaining the largest normalized DBP is relatively high. For applications that desire very low GVD, the case $S_x = 0.462a$, $S_y = 0$, and $R = 0.25a$ is more appropriate despite the fact that this structure attains a lower normalized DBP value. In this case, the maximum (in absolute value) GVD value in the middle region of two zero points is 5.54×10^2 in terms of normalized units. That number corresponds to approximately 0.32 ps^2/mm if it is multiplied by a coefficient of $a/2\pi c^2$. The need to achieve a minimum GVD in the present case puts a constraint on the bandwidth of the input pulse. By inspection, this frequency interval is [0.2135,0.2143] $2\pi c/a$, corresponding to a relative bandwidth ($\Delta\omega/\omega_c$) of 0.3% and a bandwidth of 5.5 nm. In this frequency range, the maximum (absolute value) TOD value of the relevant band is 5.53×10^6 in terms of normalized units. It turns out to be 0.572 ps^3/mm if a multiplication coefficient of $a^2/4\pi^2c^3$ is used.

Finally, we emphasize that the parameter optimization discussed in Section 2 is not fully complete. For example, a scanning of R should also be performed for other S_x values. Indeed, we also scanned various S_x and R values for the case of $S_x = 0.50a$. It is revealed that normalized DBP can be enhanced up to 0.554 for the following parameters: $S_x = 0.50a$, $S_y = 0$, and $R = 0.262a$. This is the highest normalized DBP value reported according to the best of the authors' knowledge. The corresponding group index spectra for various

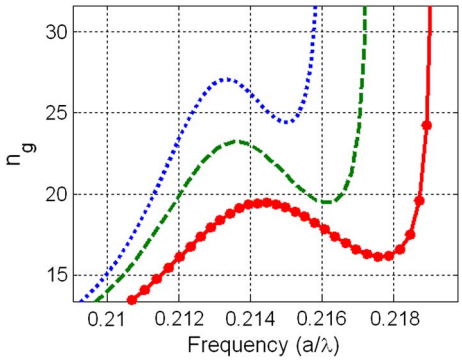

Fig. 9. (Color online) Results of additional optimization for large normalized DBP numbers. The dotted curve corresponds to the structure with parameters $S_x = 0.470a$, $S_y = 0$, $R = 0.25a$, and normalized DBP = 0.441. The dashed curve corresponds to the structure with parameters $S_x = 0.478a$, $S_y = 0$, $R = 0.254a$, and normalized DBP = 0.518. The curve with circles corresponds to the structure with the following parameters: $S_x = 0.500a$, $S_y = 0$, $R = 0.262a$, DBP = 0.554.

cases are given in Fig. 9. Here, it should be stated that if the normalized DBP calculation criteria is changed, then the optimum normalized DBP value will be obtained by a different set of parameters. This is due to the fact that local minima and maxima of S-shaped lobes should obey the new percentage criterion adapted for the group index spectrum.

The reported normalized DBP based on 2D analysis is fairly high compared to the majority of slow light scenarios, which report numbers around 0.25–0.30. Normalized DBP value over 0.50 has not been reported yet to the best of authors' knowledge. In order to ensure that the maximum normalized DBP is achieved at $R = 0.262a$ and $S_x = 0.50a$, we performed scanning of S_x and R in the vicinity of the optimized values. The scanning result is presented in Fig. 10. We found the maximum normalized DBP value at $S_x = 0.50a$ and $R = 0.262a$ after we scanned various S_x and R values with steps of $0.004a$ ($0.484a \le S_x \le 0.500a$) and ($0.250a \le R \le 0.298a$). We can see in Fig. 10 that there is an optimum S_x for a specific R value and vice versa. Among these optimum numbers, the best case that provide largest normalized DBP corresponds to $S_x = 0.50a$ and $R = 0.262a$.

An important concern with the slow light PC waveguide is the loss due to possible disorder. It is expected that the

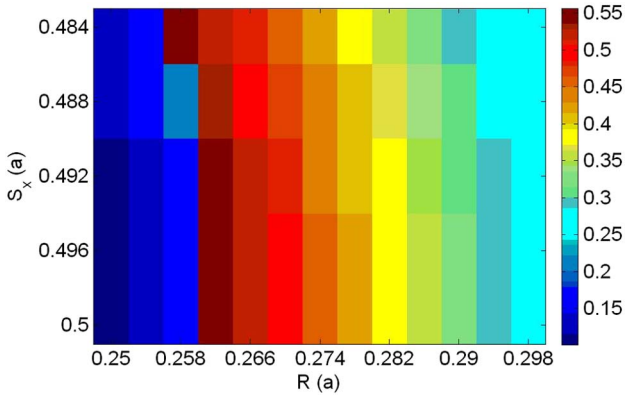

Fig. 10. (Color online) Parameter scan in the vicinity of the values that provide the largest normalized DBP value. The sharp decay on the left side of the graph is due to the fact that the S-shaped group index spectrum does not satisfy the ±10% criteria.

disorder on the holes lying along the waveguide centerline may affect the operation of the structure. To discuss the effect of the perturbed centered holes on the loss factor, we carried out 2D finite-difference time-domain (FDTD) simulations. The grid size of the computational domain is $a/40$. The central holes' radii on the centerline deviate from the mean value by 2 nm (the distribution of the radii is Gaussian). The analyzed structure has an average group index value of 17.82 (Fig. 9, the curve with circles). The section of the waveguide with disorder is $40a$. The frequency content of the incident Gaussian modulated sinusoidal wave is tuned to the nearly constant group index frequency interval [center frequency $\omega_c = \frac{a}{\lambda} = 0.2154$ with a frequency bandwidth of $\Delta\omega = 6.73 \times 10^{-3}(2\pi c/a)$]. The findings show that the loss due to that specific type of disorder is 0.012 dB/μm for standard deviation of 2 nm. The other loss factors, such as three-dimensional (3D) radiation loss and the disorder loss due to side holes, are not taken into account in this analysis. We should note that the targeted constant frequency window has a moderate group index. Hence, the reported loss parameters are tolerable.

The 3D version of the structure (2D PC slab suspended in air) is also taken into consideration. The structure is analyzed with a plane wave expansion method with a grid size of $a/30$. The slab thickness is taken to be $h = 0.7a$. We obtained a DBP of 0.511 for the structural parameters $S_x = 0.500a$, $R = 0.236a$, and $r = 0.30a$. The parameters found in the 2D analysis did not give the highest normalized DBP for the 3D case as expected. Therefore, by a brief scanning of the parameter R, we achieve a normalized DBP of 0.511 with a slightly different set of values. The group index spectra obtained in the 3D analysis is given in Fig. 11. One expected change that occurs in the 3D analysis is the movement of the dispersion band to higher values. In addition, the normalized DBP value slightly decreases.

Additionally, a loss analysis can also be performed based on the above-mentioned PC waveguide slab with a finite height. The loss analysis performed previously by 2D FDTD ignores the role of out-of-plane losses. To analyze the loss in more detail, with the inclusion of the first, second, and third rows of holes in addition to the central row of holes, we have followed an approach presented in [32]. It should be noted that the out-of-plane loss is also considered in this calculation. The results reveal that the loss can be approximated to 0.028 dB/μm on average, as shown in Fig. 12. The out-of-plane loss and in-plane loss parts can be separated as 0.0018 dB/μm and 0.0262 dB/μm, respectively. The 3D structure attains an

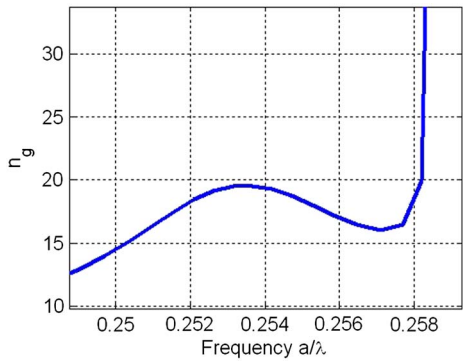

Fig. 11. (Color online) Group index spectra of the three-dimensional slow light photonic structure.

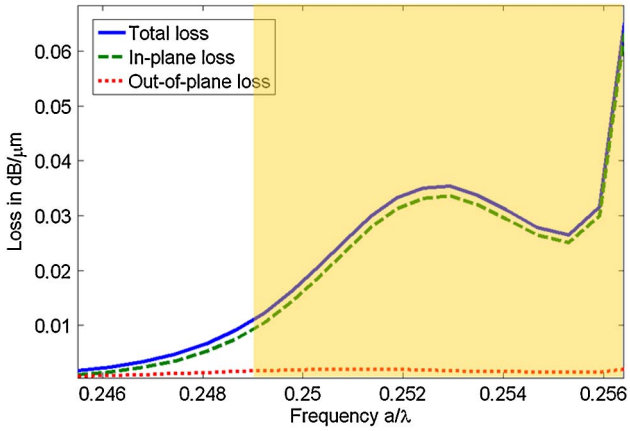

Fig. 12. (Color online) In-plane loss, out-of-plane loss, and total loss. The shaded region shows the region of interest. There is a sharp increase in loss where the frequencies are closer to the band edge.

average group index value of 17.78. The in-plane loss value is roughly three times larger than the number obtained by the 2D FDTD result. This is due to the fact that in the FDTD simulations we only analyzed the disorder due to the perturbations of the central row of holes. The remarkable observation that can be made from Fig. 12 is that the out-of-plane loss is fairly small compared to the in-plane loss. This result is also consistent with the prospect that the slow mode stays below the light line and, therefore, the out-of-plane losses will be small. In the present analysis, we also added the effects of the first, second, and third rows and their impact on the out-of-plane scattering. Hence, it is not unexpected that the total loss should be larger than the one reported with the 2D FDTD.

6. CONCLUSION

In this study, we demonstrate a new 2D PC waveguide configuration with uniquely enhanced DBP and GVD properties. This structure consists of a standard triangular lattice PC, but a line defect is imposed by changing the radius and location of the holes that occupy the waveguide centerline. By structural optimizations, a normalized DBP of 0.554 is obtained. The structure is also investigated in 3D, and a normalized DBP of 0.511 is found with a slightly different set of parameters. To the best of the authors' knowledge, these values are the highest values achieved with PC waveguides. We also propose a structure with different parameter values that attains better GVD characteristics with a lower normalized DBP. Compared with the literature, our structure has low GVD values.

To summarize, in this article it is demonstrated that this type of line defect photonic waveguide structure can attain exceptionally good slow light performance if the needed modifications are carried out. We believe this study will expand the horizons of slow light researchers and increase the usability of such waveguides in optical buffers, sensors, and nonlinear optics [33,34].

ACKNOWLEDGMENTS

The authors gratefully acknowledge the financial support of the Scientific and Technological Research Council of Turkey (TUBITAK), project numbers 108T717 and 110T306. H. Kurt also acknowledges support from the Turkish Academy of Sciences Distinguished Young Scientist Award (TUBA-GEBIP).

REFERENCES

1. E. Yablonovitch, "Inhibited spontaneous emission in solid-state physics and electronics," Phys. Rev. Lett. **58**, 2059–2062 (1987).
2. S. John, "Strong localization of photons in certain disordered dielectric superlattices," Phys. Rev. Lett. **58**, 2486–2489 (1987).
3. J. D. Joannopoulos, S. G. Johnson, R. D. Meade, and J. N. Winn, *Photonic Crystals: Molding the Flow of Light*, 2nd ed. (Princeton University, 2008).
4. J. B. Khurgin and R. S. Tucker, eds., *Slow Light: Science and Applications* (CRC, 2009).
5. L. H. Frandsen, A. V. Lavrinenko, J. Fage-Pedersen, and P. I. Borel, "Photonic crystal waveguides with semi-slow light and tailored dispersion properties," Opt. Express **14**, 9444–9450 (2006).
6. H. Kurt, H. Benisty, T. Melo, O. Khayam, and C. Cambournac, "Slow-light regime and critical coupling in highly multimode corrugated waveguides," J. Opt. Soc. Am. B **25**, C1–C14 (2008).
7. J. Li, T. P. White, L. O'Faolain, A. Gomez-Iglesias, and T. F. Krauss, "Systematic design of flat band slow light in photonic crystal waveguides," Opt. Express **16**, 6227–6232 (2008).
8. H. Kurt, K. Üstün, and L. Ayas, "Study of different spectral regions and delay bandwidth relation in slow light photonic crystal waveguides," Opt. Express **18**, 26965–26977 (2010).
9. D. Mori and T. Baba, "Wideband and low dispersion slow light by chirped photonic crystal coupled waveguide," Opt. Express **13**, 9398–9408 (2005).
10. A. Yariv, Y. Xu, R. K. Lee, and A. Scherer, "Coupled-resonator optical waveguide: a proposal and analysis," Opt. Lett. **24**, 711–713 (1999).
11. K. Üstün and H. Kurt, "Ultra slow light achievement in photonic crystals by merging coupled cavities with waveguides," Opt. Express **18**, 21155–21161 (2010).
12. A. Y. Petrov and M. Eich, "Zero dispersion at small group velocities in photonic crystal waveguides," Appl. Phys. Lett. **85**, 4866–4868 (2004).
13. A. Säynätjoki, M. Mulot, J. Ahopelto, and H. Lipsanen, "Dispersion engineering of photonic crystal waveguides with ring-shaped holes," Opt. Express **15**, 8323–8328 (2007).
14. M. Ebnali-Heidari, C. Grillet, C. Monat, and B. J. Eggleton, "Dispersion engineering of slow light photonic crystal waveguides using microfluidic infiltration," Opt. Express **17**, 1628–1635 (2009).
15. L. Dai and C. Jiang, "Ultrawideband low dispersion slow light waveguides," J. Lightwave Technol. **27**, 2862–2868 (2009).
16. D. Wang, J. Zhang, L. Yuan, J. Lei, S. Chen, J. Han, and S. Hou, "Slow light engineering in polyatomic photonic crystal waveguides based on square lattice," Opt. Commun. **284**, 5829–5832 (2011).
17. J. Ma and C. Jiang, "Demonstration of ultraslow modes in asymmetric line-defect photonic crystal waveguides," IEEE Photon. Technol. Lett. **20**, 1237–1239 (2008).
18. J. Hou, H. Wu, D. S. Citrin, W. Mo, D. Gao, and Z. Zhou, "Wideband slow light in chirped slot photonic-crystal coupled waveguides," Opt. Express **18**, 10567–10580 (2010).
19. S. Rawal, R. K. Sinha, and R. M. De La Rue, "Slow light miniature devices with ultra-flattened dispersion in silicon-on-insulator photonic crystal," Opt. Express **17**, 13315–13325 (2009).
20. M. L. Povinelli, S. G. Johnson, and J. D. Joannopoulos, "Slow-light band-edge waveguides for tunable time delays," Opt. Express **13**, 7145–7159 (2005).
21. J. Liang, L-Y. Ren, M-J. Yun, X. Han, and X-J. Wang, "Wideband ultraflat slow light with large group index in a W1 photonic crystal waveguide," J. Appl. Phys. **110**, 063103 (2011).
22. O. Khayam and H. Benisty, "General recipe for flatbands in photonic crystal waveguides," Opt. Express **17**, 14634–14648 (2009).
23. L. Dai, T. Li, and C. Jiang, "Wideband ultralow high-order-dispersion photonic crystal slow-light waveguide," J. Opt. Soc. Am. B **28**, 1622–1626 (2011).
24. R. Matzen, J. S. Jensen, and O. Sigmund, "Systematic design of slow-light photonic waveguides," J. Opt. Soc. Am. B **28**, 2374–2382 (2011).
25. F. Wang, J. S. Jensen, and O. Sigmund, "Robust topology optimization of photonic crystal waveguides with tailored dispersion properties," J. Opt. Soc. Am. B **28**, 387–397 (2011).
26. S. Johnson and J. Joannopoulos, "Block-iterative frequency-domain methods for Maxwell's equations in a planewave basis," Opt. Express **8**, 173–190 (2001).
27. R. J. P. Engelen, Y. Sugimoto, Y. Watanabe, J. P. Korterik, N. Ikeda, N. F. van Hulst, K. Asakawa, and L. Kuipers, "The effect of higher-order dispersion on slow light propagation in photonic crystal waveguides," Opt. Express **14**, 1658–1672 (2006).
28. T. Baba, "Slow light in photonic crystals," Nat. Photon. **2**, 465–473 (2008).
29. R. S. Tucker, P. Ku, and C. J. Chang-Hasnain, "Delay-bandwidth product and storage density in slow-light optical buffers," Electron. Lett. **41**, 208–209 (2005).
30. T. Baba, T. Kawasaki, H. Sasaki, J. Adachi, and D. Mori, "Large delay-bandwidth product and tuning of slow light pulse in photonic crystal coupled waveguide," Opt. Express **16**, 9245–9253 (2008).
31. S. A. Schulz, L. O'Faolain, D. M. Beggs, T. P. White, A. Melloni, and T. F. Krauss, "Dispersion-engineered slow light in photonic crystals: a comparison," J. Opt. **12**, 104004 (2010).
32. L. O'Faolain, S. Schulz, D. M. Beggs, T. P. White, L. Spasenovic, L. Kuipers, F. Morichetti, A. Melloni, J. Mazoyer, P. Hugonin, P. Lalanne, and T. F. Krauss, "Loss engineered slow light waveguides," Opt. Express **18**, 27627–27638 (2010).
33. K. H. Jensen, M. N. Alam, B. Scherer, A. Lambrecht, and N. A. Mortensen, "Slow-light enhanced light-matter interactions with applications to gas sensing," Opt. Commun. **281**, 5335–5339 (2008).
34. C. Monat, M. de Sterke, and B. J. Eggleton, "Slow light enhanced nonlinear optics in periodic structures," J. Opt. **12**, 104003 (2010).